

Spectral Hong–Ou–Mandel Interference between Independently Generated Single Photons for Scalable Frequency-Domain Quantum Processing

Anahita Khodadad Kashi and Michael Kues*

The photon's frequency degree of freedom, being compatible with mature telecom infrastructure, offers large potential for the stable and controllable realization of photonic quantum processing applications such as the quantum internet. The Hong–Ou–Mandel effect, as a two-photon interference phenomenon, serves as a central building block for such frameworks. A key element yet missing to enable meaningful frequency-based implementations as well as scalability in the number of processed photons, is the demonstration of the Hong–Ou–Mandel effect between independently created photons of different frequencies. The experimental implementation of bosonic and fermionic frequency domain Hong–Ou–Mandel interference between independently generated single photons is reported here, with measured visibilities of $74.31\% \pm 3.56\%$ and $86.44\% \pm 8.27\%$, respectively. This is achieved through a scalable photonic frequency circuit that creates two post-selected pure single photons, which undergo frequency mixing at an electro-optic phase modulator. The system is on-the-fly reconfigurable allowing to probe bosonic and fermionic Hong–Ou–Mandel interference in the same experimental setup. The work demonstrates the versatility of frequency domain processing and its scalability toward higher photon numbers, which enables new quantum gate concepts as well as the establishment of frequency-based large-scale quantum networks.

high-dimensional states with an in turn better noise resilience.^[2,3] Specifically, the frequency domain approach is compatible with well-developed omnipresent optical telecommunication infrastructure such as fiber networks, wavelength division de/multiplexers, electro-optic phase modulators (EOPM), and programmable filters, whose standard single-spatial-mode operation preserves phase stability. In contrast to polarization or time-mode encoding, which are accompanied with instabilities for large fiber distances, the frequency domain is advantageous and hence particularly suited for, e.g., the quantum internet. Furthermore, the controllability of programmable filters as well as the reconfigurability of EOPMs through adjusting the radio frequency (rf) modulation, can alleviate the circuit complexity, which is strictly required for large-scale implementations of quantum applications.


The Hong–Ou–Mandel (HOM) interference effect, which manifests as the bunching (bosonic)/antibunching

(fermionic) of two indistinguishable photons upon mixing at a mode splitter,^[4] is central to quantum computation,^[5] nonclassical communication,^[6,7] and quantum-enhanced metrology.^[8] Quantum random walks,^[9] boson sampling,^[10] linear optical quantum gates,^[11–13] and quantum dense coding^[14] are a few examples where the HOM effect is ubiquitously exploited. In

1. Introduction

Photonic frequency encoding of quantum information can realize the stable and controllable implementation of quantum processing by the use of state-of-the-art telecommunication infrastructure^[1] and at the same time it gives access to robust

A. Khodadad Kashi, Prof. M. Kues
Institute of Photonics
Leibniz University Hannover
Nienburger Str. 17, Hannover 30167, Germany
E-mail: michael.kues@iop.uni-hannover.de

 The ORCID identification number(s) for the author(s) of this article can be found under <https://doi.org/10.1002/lpor.202000464>

© 2021 The Authors. Laser & Photonics Reviews published by Wiley-VCH GmbH. This is an open access article under the terms of the Creative Commons Attribution-NonCommercial-NoDerivs License, which permits use and distribution in any medium, provided the original work is properly cited, the use is non-commercial and no modifications or adaptations are made.

DOI: 10.1002/lpor.202000464

A. Khodadad Kashi, Prof. M. Kues
Hannover Centre for Optical Technologies
Leibniz University Hannover
Nienburger Str. 17, Hannover 30167, Germany

A. Khodadad Kashi, Prof. M. Kues
Cluster of Excellence PhoenixD (Photonics, Optics, and Engineering – Innovation Across Disciplines)
Leibniz University Hannover
Hannover 30167, Germany

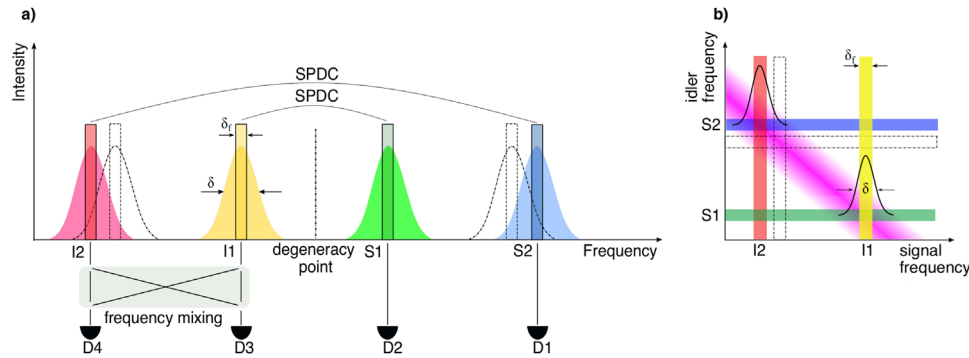


Figure 1. Schematic outline of the concept for frequency domain HOM interaction between two pure and independently created photons I1 and I2: a) The four photons produced out of two SPDC processes are created with a single-mode bandwidth δ (indicated by Gaussian shaped graphics) that is accessible with common telecommunication filters. Spectral filters defining four frequency modes S1, S2, I1, and I2 with a bandwidth of δ_f are represented by rectangular shapes. The frequency mixing is applied on I1 and I2, whereupon the four-fold coincidence detection on D1, D2, D3, and D4 allows for the HOM interference to occur. The dash-dotted spectral profiles represent an alternative filter setting for I1 and S1 which, due to the overlap of the single frequency mode bandwidth, adds to the background noise. b) Sketch of the joint spectral intensity function of the two-photon states (pink) with indicated filter positions according to (a).

quantum key distribution protocols, the HOM visibility reveals the success probability of the secret key rate^[6,15] and in quantum repeaters, quantum teleportation is performed dependently on projective Bell-state measurements realized via HOM interference.^[16] However, to date implementations have mainly employed spatial domain HOM interference,^[17] for which additional number of waveguides and a control over several different arrangements are required to meet large-scale real-world implementations.

Frequency-domain HOM interference between a single photon and a coherent state was realized using optical nonlinear parametric effects as a means for frequency mixing,^[18] which however required complex bulk optical setups and suffered interferometric degradation as a result of multi-photon generation. Moreover, an HOM effect was shown between two photons created from a continuous-wave-excited spontaneous parametric down conversion (SPDC) process where an EOPM was utilized as a frequency mixer,^[19] which is limited in scalability, i.e., it cannot be extended to higher numbers of involved photons in the system due to the inherent spectral impurity of the photons. In order to enable an HOM effect between independently generated single photons and in turn to provide scalability, the preparation of spectrally pure single photons is highly indispensable.

In the present work, we use a novel approach, employing a pulsed excitation field, an EOPM, and programmable filters, to demonstrate for the first-time frequency-domain bosonic and fermionic HOM interference between two independently generated single photons.

In this work, the bosonic and fermionic HOM effects are demonstrated with measured visibilities of $74.31\% \pm 3.56\%$ and $86.44\% \pm 8.27\%$, respectively; the obtained values fall well beyond the classical limit of 50% offering an appropriate candidate for quantum communication and information applications. In addition, the feasibility of switching between the bosonic and fermionic HOM effect extends the versatility of this quantum platform, necessary, e.g., to enhance the performance of quantum gates.^[13]

2. Frequency Domain HOM Concept and Experimental Setup

Two or more frequency bins can be mixed using an rf-driven EOPM, if their generated sidebands spectrally overlap. Such principal of operation suggests that an EOPM can be considered as a frequency-domain analog of a conventional spatial beam splitter, in turn allowing for HOM interference in the frequency domain. In this context, two photons in two different frequency modes simultaneously (within the reciprocal spectral bandwidth of the associated fields) arrive at the EOPM and mix. Depending on the relative phase of the involved sidebands being π or 0, the photons coalesce either in the same frequency mode (bunching phenomenon), in turn leading to zero coincidence detection and an interferometric dip (bosonic HOM), or each ends up in one of the two different frequency modes (antibunching phenomenon), resulting in enhanced coincidence detection and an interferometric peak (fermionic HOM).

To demonstrate the bosonic and fermionic frequency domain HOM effect for two independently created photons, we followed the concept explained schematically in **Figure 1**; photon pairs were generated through a spontaneous parametric down-conversion process, where one excitation photon is annihilated and two new photons, named signal and idler, are created simultaneously. In this work, two SPDC processes are considered, producing two pairs of photons within one excitation pulse. Two pairs of spectrally separated signal and idler frequency bins were defined, with one pair labeled as S1 (green) and I1 (yellow) and the other as S2 (blue) and I2 (red). This approach creates the following state: $|\psi\rangle_{2\text{SPDC}} = \frac{1}{\sqrt{3}} (|1_{I2}, 1_{I1}, 1_{S1}, 1_{S2}\rangle + |2_{I2}, 0_{I1}, 0_{S1}, 2_{S2}\rangle + |0_{I2}, 2_{I1}, 2_{S1}, 0_{S2}\rangle)$ ^[20] with the first term emerging from two SPDC processes radiating into different frequency bins whereas the last two terms describe the emission into the same pair of frequency bins. The detection of photons in S1 and S2 projects the state $|\psi\rangle_{2\text{SPDC}}$ into $|\psi\rangle_{\text{in}} = |1_{I1}, 1_{I2}\rangle$, giving access to two independently generated single photons in the idler I1 and I2 frequency bins. Frequency mixing applied to the ultimate post-selected state allows for the HOM effect to take place.

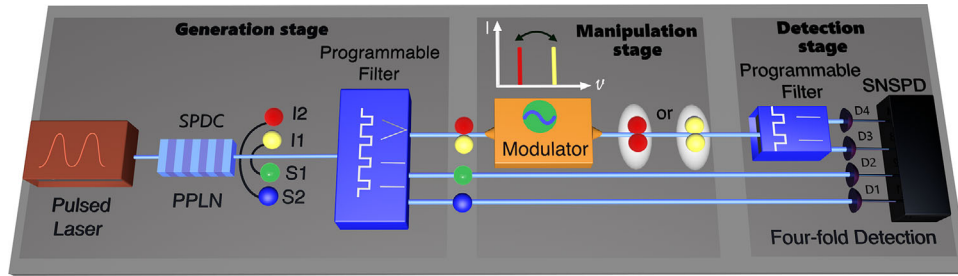


Figure 2. Schematic illustration of the experimental setup employed for demonstrating the frequency domain HOM effect of two independently created photons. See the text for details.

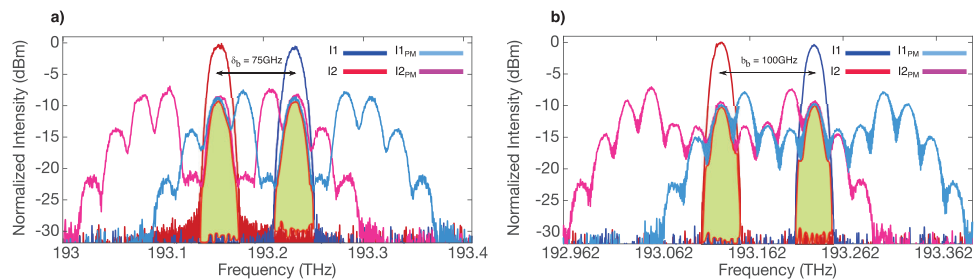


Figure 3. Classically measured spectrum of the defined idler components before and after modulation: a) bosonic case with 75 GHz frequency spacing set between the idler modes, where the phase-modulated third- and the zeroth-order sidebands superimpose, and b) fermionic case with 100 GHz frequency spacing between the idler components, set to enable the phase-modulated fourth and zeroth-order sidebands to superimpose. The shaded area indicates the overlap of the respective sidebands. With an EOPM insertion loss of 2.8 dB, a total transmission for the 2-by-2 splitter of 16.64% and 12.26% was measured for the bosonic and fermionic settings, respectively.

The experimental setup presented in **Figure 2** was employed to this end.

A mode-locked pulsed laser with a center wavelength of ≈ 775 nm and filtered to a bandwidth of ≈ 200 GHz, was coupled into a periodically poled lithium niobate waveguide (type-0 quasi-phase-matched, 40 mm long, 5% MgO-doped). Two SPDC processes create, out of the excitation field, two pairs of correlated photons around 1550 nm. A programmable filter was used to define the two pairs of spectrally separated signal and idler frequency bins each with a bandwidth of 22 GHz, allowing for ≈ 14 kHz single photon detection rate (linearly dependent on the filter bandwidth). The two signal components S1 and S2 were directed through different ports of the first programmable filter toward two superconducting nanowire single photon detectors D2 and D1, respectively. The two idler photons were directed to an EOPM where the frequency mixing led to the occurrence of frequency domain HOM interference. A second programmable filter was employed to split the frequency bins I1 and I2, leading to detections on D3 and D4.

To probe bosonic and fermionic HOM effects, different filter and modulation configurations were applied within the same experimental setup; the EOPM was driven by an rf tone of $\Omega = 25$ GHz (maximal operation frequency of the used RF amplifier) and the amplitude of the modulation signal was judiciously set in each case so as to provide the required identical splitting amplitude between the zeroth order (fundamental) and the considered higher-order sidebands (for more details see the Experimental Section). To probe a bosonic HOM effect, the signs in the mixing process of the frequency modes need to differ. Such a sign difference is present when the third-order sidebands are

selected for the mixing process, requiring the frequency spacing of the idler bins to be set at 75 GHz. In contrast, to investigate the fermionic HOM effect, the signs in the mode mixing need to be equal, which can be achieved by choosing the fourth-order sidebands for the mixing process, requiring the idler bin spacing to be adjusted at 100 GHz. **Figure 3** shows the classically measured spectral response of the EOPM for both the bosonic and fermionic cases.

A high spectral purity of the two independently created photons is crucial to obtain a high degree of visibility in their HOM interaction. The purity is inversely related to the number of effective frequency modes the photon contains,^[21] which can be controlled by spectral filtering the signal and idler fields.^[22] In our experimental setup, a pulsed excitation bandwidth of 200 GHz together with a phase matching bandwidth of 55 GHz was selected such that the minimal arrangeable bandwidth of the programmable filter (20 GHz) allowed to prepare photons with a single frequency mode. In this regard, a Hanbury-Brown and Twiss (HBT) experiment was performed to measure the number of frequency modes as a function of the filter bandwidth. Specifically, the idler I1 mode was split 50:50 with the programmable filter and sent to two detectors, to measure the second-order autocorrelation function $g^2(0) = 1 + p = 1 + 1/k$, with p and k denoting the spectral purity and the number of Schmidt modes, respectively.^[21] A $g^2(0)$ with a value of 2 corresponds to the spectrally pure case, i.e., $k = 1$, whereas theoretical infinite number of modes $k = \infty$ establishes a lower limit of 1 for $g^2(0)$. The dependency of the second-order autocorrelation function $g^2(0)$ and the number of Schmidt modes k on the spectral bandwidth are shown in **Figure 4**. A theoretical model^[21] fits

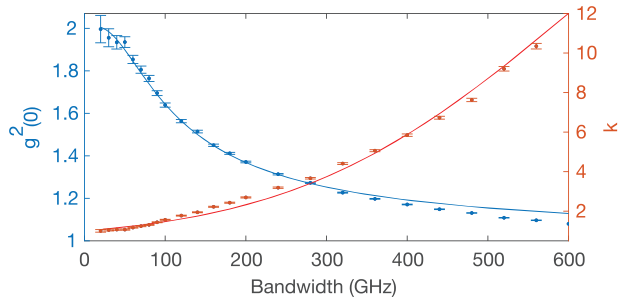


Figure 4. Dependency of the second-order autocorrelation function $g^2(0)$ and the number of frequency modes k on the spectral bandwidth, obtained from the HBT experiment. The experimental data fit well to a theoretical model (solid lines) that considers a Gaussian spectral filtering bandwidth.^[21] The error bars correspond to standard deviation associated with 10 min integration time per measurement.

well with the experimental data (solid line) and allowed to determine the single-frequency-mode bandwidth, that is 55 GHz. A maximum spectral purity of $p = 99.65\% \pm 6.5\%$, corresponding to $k = 1.0035 \pm 0.065$, is obtained at 20 GHz. It is worth to mention that a narrow-band continuous wave-excited SPDC process would not allow to prepare single-frequency-mode photons, for, in that case the single-mode bandwidth is much narrower (in order of kHz) than the filtering capability offered by today's elaborated filtering techniques. This highlights the importance of a pulsed excitation field.

The capability of the programmable filter in defining two coexistent spectral transmission regions allowed to create two single-frequency mode photons within the same spatial mode. The selection of idler frequency bins requires at its minimum a

center-to-center frequency spacing of a single-frequency mode bandwidth, so as to suppress the unwanted coincidence counts in the detection of photons in S1 and I2 as well as S2 and I1, emerging from off-diagonal spurious spectrally correlated regions (see Figure 1b, dash-dotted filter settings for I1 and S1). This condition was achieved at 75 GHz ($\approx 1.35 \times$ single mode bandwidth) and 100 GHz (approximately twice the single mode bandwidth) for the bosonic and fermionic cases, respectively.

3. Frequency-Domain HOM Results

Fourfold coincidence detection was performed for the bosonic and fermionic settings, as stated previously, where the pulsed excitation provided the required precise timing between the two pairs. Specifically, the creation of the two idler photons I1 and I2 in the same excitation pulse and their spectral filtering led to their simultaneous and thus temporally indistinguishable arrival at the EOPM splitter, in turn leading to the HOM effect (interactive case). In contrast, two idler photons each originating from a different excitation pulse were temporally distinguishable at the EOPM splitter and as a result no HOM interaction took place (noninteractive cases). Time-multiplexed fourfold post-processing considering different pulse periods between the idler photons was exploited to distinguish these cases.

Fourfold coincident counts as function of different pulse periods are shown in Figure 5a,b for enabled frequency splitting (modulation enabled) and in Figure 5c,d for disabled splitting (modulation disabled). For the bosonic setting, shown in Figure 5a, an HOM dip with a visibility of $74.31\% \pm 3.57\%$ was observed for active splitting. Here, the visibility was determined by $V_B = (CC_{\max}^B - CC_{\min}^B) / CC_{\max}^B$, where CC_{\max}^B is the average coincidence count of the noninteractive cases and

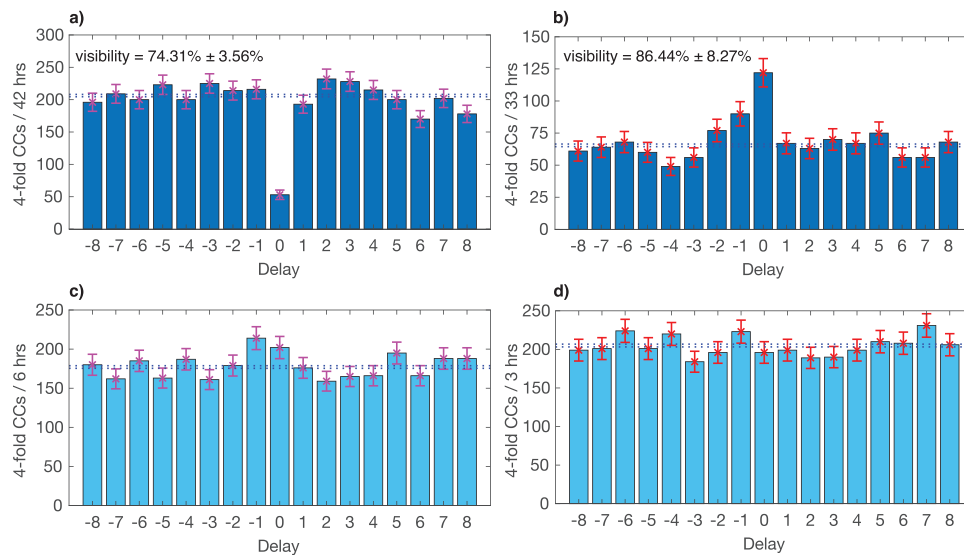


Figure 5. Post-processed fourfold coincidence counts versus pulse delay expressed in terms of multiples of the pulse period. Two-photon HOM interference pattern obtained under a) bosonic and b) fermionic experimental conditions for enabled frequency splitting. The error bars indicate standard deviation (calculated as the square root of the four-photon coincidence counts) corresponding to the integration time of each measurement, labeled on the vertical axis of the diagrams. For disabled frequency splitting but otherwise same experimental conditions, the coincidence counts versus different pulse periods are shown for the bosonic and fermionic configurations in panels (c) and (d), respectively. In all four panels, the dotted horizontal lines represent the average counts for the noninteracting cases. The bosonic and fermionic measurements were performed under 160 and 190 μ W excitation power, respectively.

CC_{\min}^B is the coincidence count of the interactive case. For the fermionic setting, displayed in Figure 5b, an HOM peak with a visibility of $86.44\% \pm 8.27\%$ was obtained, calculated through $V_F = (CC_{\max}^F - CC_{\min}^F)/CC_{\min}^F$, with CC_{\min}^F being the average count of the noninteractive cases and CC_{\max}^F the count of the interactive case. By simply turning off the modulator, a measurement with disabled splitting was performed, see Figure 5c,d, where no HOM interaction was found, further validating that the previously obtained interferometric dip and peak were due to frequency mixing and in turn the HOM effect.

A characterization of the HOM interference shape in the frequency domain, by adjusting the frequency overlap through an RF frequency scan, is precluded as in that case the frequency dependency of the RF amplification affects the splitting ratio of the frequency mixer.

HOM visibility degrades as a result of experimental imperfections, among which are the spectral profile mismatch between the interacting frequency modes, the unequal spectral splitting ratio of the involved sidebands and background terms $|2, 0, 1\rangle_{bg}$ and $|0, 2, 1\rangle_{bg}$, emerging from both spurious correlations and higher-order SPDC processes (not leading to HOM interference).

In order to have a quantitative estimate over the imperfection contributions, the classical measurements presented in Figure 3 were considered, where we calculated a 90.96% and 97.75% spectral overlap between the fundamental and considered sidebands, i.e., the 0th and ± 3 rd as well as the 0th and ± 4 th, respectively. Furthermore, 4% deviation from perfect 50:50 frequency mixing ratio was measured for both the bosonic and fermionic case. As an additional degradation factor, we characterized the input state $|\psi\rangle_{in} = \alpha|1, 1, 1, 1\rangle_S + \beta|2, 0, 1, 1\rangle_{bg} + \gamma|0, 2, 1, 1\rangle_{bg}$ to determine the coefficients of the background (β and γ) to the ideal input state (α) by performing fourfold coincidence detection with no phase modulation process applied. For the bosonic setting, we obtained $\alpha_B = 0.9945$, $\beta_B = 0.0727$, and $\gamma_B = 0.0587$, whereas for the fermionic setting, we found $\alpha_F = 0.9920$, $\beta_F = 0.0826$, and $\gamma_F = 0.0958$. The slightly higher background values in the fermionic case can be explained by higher excitation powers which subsequently lead to higher multi-photon generation rates. Considering the background terms in the HOM treatment,^[21] the corresponding degradations in the visibility were 1% and 1.5% in bosonic and fermionic HOM effects, respectively. The sum of the degradation contributions in both cases thus explains the deviation of the measured visibilities from ideal 100%.

4. Conclusion

In this work, we demonstrated the frequency-domain implementation of HOM interference between independently created single photons. A combination of pulsed excitation, reconfigurable electro-optic phase modulator, and programmable filters enabled a controllable photonic frequency circuit, which is not found in previously presented HOM implementations. The measured interferometric visibilities fell beyond the classical limit, required for quantum information processing. The added reconfigurability enabled bosonic and fermionic HOM effects within the same experimental setup which can be used, e.g., for functionality adaptation of quantum logic gates as well as preparing antisymmetric Bell states,^[13] thus highlighting the versatility and

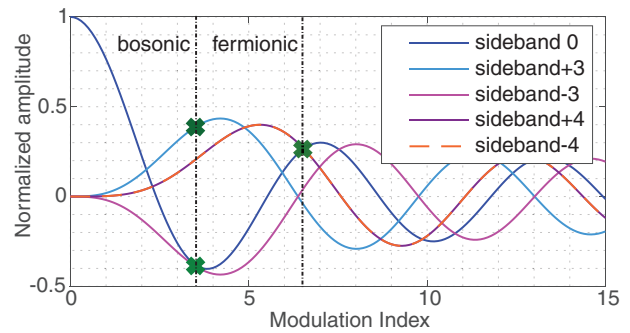


Figure 6. Simulations of sideband generation in the electro-optic phase modulation process. The sidebands are expressed as Bessel functions of n th order ($n = 0, \pm 3, \pm 4$). The left and right black dotted lines indicate modulation depths well suited to bosonic and fermionic HOM conditions, respectively.

potential of the frequency domain approach. As important, our results enable the scalability of frequency domain processing to higher numbers of photons, e.g., allowing fundamental Bell-state measurement in the frequency degree-of-freedom. Larger multi-chromatic multi-photon states can be achieved by defining additional filter functions and adding to the number of single photon detectors. In this regard, the capability of the EOPM as a frequency mixer can be extended from a 2-by-2 to an N -by- N splitter by considering further sidebands, which increases transmission and gives access to richer photon interactions. To improve detection rates and overall performance, the EOPM process can be optimized by, e.g., the use of more complex modulation functions as well as the concatenation of modulators^[23] and the integration of the presented scheme on photonic chips. Our work thus allows for the practical and meaningful frequency-domain implementation of fundamental concepts, such as entanglement swapping, teleportation, and novel complex gates, which are at the basis of future quantum networks as well as the creation of frequency-based complex states for quantum metrology applications.

5. Experimental Section

Sideband Selection for Bosonic and Fermionic HOM Photon Statistics: A single-frequency component at ω_0 is phase modulated at an rf tone Ω , and thereafter it expands into n number of equally spaced sidebands, which are generated at frequencies $\omega_0 \pm n\Omega$ with their amplitudes expressed as Bessel functions of the first kind $J_n(\mu)$.^[24] The probability amplitude of different sidebands can be controlled via tuning the modulation index μ , defined as the ratio of the peak amplitude V_m of the modulating signal to the half-wave voltage V_π of the electro-optic modulator. For different sideband orders n , the following relation holds true: $J_{-n}(\mu) = (-1)^n J_n(\mu)$, highlighting a π phase shift between positive and negative sidebands with odd order.

In order to realize an equal mixing ratio, the modulation setting should be adapted such that the post modulation amplitude of the original frequency component is identical to that of the generated sidebands with which its frequency mixing is targeted. In Figure 6, calculations demonstrating the variations in the normalized amplitude of the n th-order sidebands (here $n = 0, \pm 3, \pm 4$) as function of different modulation indices is shown; it was observed that at specific modulation depths the intensity in the original frequency bin, referred to as the 0 phase-modulated sideband, equals that of the third order sidebands with a relative π phase difference between +3 and -3. The same is observed for 0 and fourth sidebands, but with a 0 relative phase between +4 and -4.

The π phase difference between ± 3 sidebands (similar to the phase flip of a spatial beam splitter) leads to the cancelation of transmission and reflection probability amplitudes for a two-photon input. Here, the transmission probability amplitude refers to the zeroth-order sideband whereas the reflection probabilities are represented by third-order sidebands. This would in turn result in the formation of an interferometric dip, the whole process being the bosonic HOM effect. In contrast, the relative 0 phase difference between ± 4 sidebands contributed to constructive interference between the transmission and reflection probability amplitudes, thereby creating an interferometric peak, representing the fermionic HOM interference.

Note that sideband creation outside the computational domain can be overcome by, e.g., concatenation of phase modulators and programmable filters,^[23] where state transmission of close to 100% can be achieved.

Experimental Setup Characteristics: The EOPM had an insertion loss of 2.8 dB. The RF amplifier operational range was 18–26 GHz. The programmable filter had a minimum arrangeable bandwidth of ≈ 20 GHz with an extinction ratio of 50 dB and an insertion loss of 4.5 dB. For reference, the measured two-photon signal-idler coincidence rate in the HOM measurement were 173.5 and 107 Hz for the bosonic and fermionic case, respectively.

Acknowledgements

The authors acknowledge funding from the German Federal Ministry of Education and Research, Quantum Futur Program (PQuMAL). The authors kindly thank Bernhard Roth for lending an experimental equipment.

Open access funding enabled and organized by Projekt DEAL.

Conflict of Interest

The authors declare no conflict of interest.

Data Availability Statement

Research data are not shared.

Keywords

bi-chromatic two-photon state, Hong–Ou–Mandel interference, independently generated single photons, photonic frequency-domain processing

Received: October 21, 2020

Revised: February 19, 2021

Published online: March 18, 2021

- [1] M. Kues, C. Reimer, J. M. Lukens, W. J. Munro, A. M. Weiner, D. J. Moss, R. Morandotti, *Nat. Photonics* **2019**, *13*, 170.
- [2] J. Nunn, L. J. Wright, C. Söller, L. Zhang, I. A. Walmsley, B. J. Smith, *Opt. Express* **2013**, *21*, 15959.
- [3] M. Kues, C. Reimer, P. Roztocky, L. R. Cortés, S. Sciara, B. Wetzel, Y. Zhang, A. Cino, S. T. Chu, B. E. Little, D. J. Moss, L. Caspani, J. Azaña, R. Morandotti, *Nature* **2017**, *546*, 622.
- [4] C. K. Hong, Z. Y. Ou, L. Mandel, *Phys. Rev. Lett.* **1987**, *59*, 2044.
- [5] E. Knill, R. Laflamme, G. J. Milburn, *Nature* **2001**, *409*, 46.
- [6] H. K. Lo, M. C. Curty, B. Qi, *Phys. Rev. Lett.* **2012**, *108*, 130503.
- [7] F. Xu, X. Ma, Q. Zhang, H. K. Lo, J. W. Pan, *Rev. Mod. Phys.* **2020**, *92*, 025002.
- [8] A. E. Ulanov, I. A. Fedorov, D. Sychev, P. Grangier, A. I. Lvovsky, *Nat. Commun.* **2016**, *7*, 11925.
- [9] Y. Bromberg, Y. Lahini, R. Morandotti, Y. Silberberg, *Phys. Rev. Lett.* **2009**, *102*, 253904.
- [10] A. Crespi, R. Osellame, R. Ramponi, D. J. Brod, E. F. Galvão, N. Spagnolo, C. Vitelli, E. Maiorino, P. Mataloni, F. Sciarrino, *Nat. Photonics* **2013**, *7*, 545.
- [11] P. Kok, W. J. Munro, K. Nemoto, T. C. Ralph, J. P. Dowling, G. J. Milburn, *Rev. Mod. Phys.* **2007**, *79*, 135.
- [12] J. L. O'Brien, G. J. Pryde, A. G. White, T. C. Ralph, D. Branning, *Nature* **2003**, *426*, 264.
- [13] T. B. Pittman, J. D. Franson, *AIP Conf. Proc.* **2011**, *1363*, 241.
- [14] K. Mattle, H. Weinfurter, P. G. Kwiat, A. Zeilinger, *Phys. Rev. Lett.* **1996**, *76*, 4656.
- [15] H. Semenenko, P. Sibson, M. G. Thompson, C. Erven, *Opt. Lett.* **2019**, *44*, 275.
- [16] R. B. Jin, M. Takeoka, U. Takagi, R. Shimizu, M. Sasaki, *Sci. Rep.* **2015**, *5*, 9333.
- [17] R. Kaltenbaek, B. Blauensteiner, M. Zukowski, M. Aspelmeyer, A. Zeilinger, *Phys. Rev. Lett.* **2006**, *96*, 240502.
- [18] T. Kobayashi, R. Ikuta, S. Yasui, S. Miki, T. Yamashita, H. Terai, T. Yamamoto, M. Koashi, N. Imoto, *Nat. Photonics* **2016**, *10*, 441.
- [19] P. Imany, O. D. Odele, M. S. Alshaykh, H.-H. Lu, D. E. Leaird, A. M. Weiner, *Opt. Lett.* **2018**, *43*, 2760.
- [20] J. C. Howell, D. Bouwmeester, *Nature* **2001**, *412*, 887.
- [21] K. Zielnicki, K. Garay-Palmett, D. Cruz-Delgado, H. Cruz-Ramirez, M. F. O'Boyle, B. Fang, V. O. Lorenz, A. B. U'Ren, P. G. Kwiat, *J. Mod. Opt.* **2018**, *65*, 1141.
- [22] Z.-Y. J. Ou, *Multi-Photon Quantum Interference*, Springer US, Boston, MA **2007**.
- [23] H.-H. Lu, J. M. Lukens, N. A. Peters, O. D. Odele, D. E. Leaird, A. M. Weiner, P. Lougovski, *Phys. Rev. Lett.* **2018**, *120*, 030502.
- [24] P. Kumar, A. Prabhakar, *IEEE J. Quantum Electron.* **2009**, *45*, 149.